J. Fluid Mech. (1991), *vol.* 230, *pp.* 97–116
Printed in Great Britain

On identifying the appropriate boundary conditions at a moving contact line: an experimental investigation

By E. B. DUSSAN V.,[1] ENRIQUE RAMÉ[2] AND STEPHEN GAROFF[3]

[1] Schlumberger-Doll Research, Old Quarry Road, Ridgefield, CT 06877-4108, USA

[2] General Electric Company, Corporate Research and Development, Schenectady, NY 12301, USA

[3] Department of Physics, Carnegie-Mellon University, Pittsburgh, PA 15213, USA

(Received 20 May 1990 and in revised form 15 February 1991)

Over the past decade and a half, analyses of the dynamics of fluids containing moving contact lines have specified hydrodynamic models of the fluids in a rather small region surrounding the contact lines (referred to as the inner region) which necessarily differ from the usual model. If this were not done, a singularity would have arisen, making it impossible to satisfy the contact-angle boundary condition, a condition that can be important for determining the shape of the fluid interface of the entire body of fluid (the outer region). Unfortunately, the nature of the fluids within the inner region under dynamic conditions has not received appreciable experimental attention. Consequently, the validity of these novel models has yet to be tested.

The objective of this experimental investigation is to determine the validity of the expression appearing in the literature for the slope of the fluid interface in the region of overlap between the inner and outer regions, for small capillary number. This in part involves the experimental determination of a constant traditionally evaluated by matching the solutions in the inner and outer regions. Establishing the correctness of this expression would justify its use as a boundary condition for the shape of the fluid interface in the outer region, thus eliminating the need to analyse the dynamics of the fluid in the inner region.

Our experiments consisted of immersing a glass tube, tilted at an angle to the horizontal, at a constant speed, into a bath of silicone oil. The slope of the air–silicone oil interface was measured at distances from the contact line ranging between $0.013a$ and $0.17a$, where a denotes the capillary length, the lengthscale of the outer region (1511 μm). Experiments were performed at speeds corresponding to capillary numbers ranging between 2.8×10^{-4} and 8.3×10^{-3}. Good agreement is achieved between theory and experiment, with a systematic deviation appearing only at the highest speed. The latter may be a consequence of the inadequacy of the theory at that value of the capillary number.

1. Introduction

It has been recognized in recent years that fluid mechanics problems containing moving contact lines are not typical. They represent a class of problems consisting of two or more immiscible fluids, each partially covering a solid surface, whose

dynamics cannot be fully analysed using the assumptions commonly associated with incompressible, immiscible, Newtonian fluids. This is not unusual in itself; for example, many fluids are known to be non-Newtonian. Its atypical aspect arises from the fact that the inadequacy of these assumptions disappears in situations devoid of moving contact lines.

As often happens in fluid mechanics, it has been the appearance of a singularity at the moving contact line which has signalled the inappropriateness of the model cited above. However, not all problems containing moving contact lines are affected equally by the presence of this singularity. General experience has shown that the impact of the singularity usually correlates well with that of surface tension. When surface tension plays a significant role, the fluid interface needs a boundary condition at the contact line. The natural boundary condition is the specification of the *contact angle*, the angle formed between the local tangent planes of the solid surface and the fluid interface. While there is no controversy concerning the use of the contact angle as a boundary condition in the absence of fluid motion, it is impossible to use it as a boundary condition in dynamic situations owing to the presence of the singularity. Consequently, problems greatly influenced by the contact angle usually represent a class significantly affected by the presence of the singularity at the moving contact line.

The obvious question which arises concerns the necessary modifications of the model of the fluids, and or solid surface, near the moving contact line which would remove the singularity. Lack of knowledge of such a model would seem to preclude performing predictive analyses of the behaviour of fluids containing moving contact lines. One popular approach has been to alter the usual hydrodynamic model by replacing the no-slip with a slip boundary condition. Various slip boundary conditions have been tried, the most popular being the one identified by Navier in 1823 (Goldstein 1938) before the extent of the success of the no-slip boundary condition was appreciated,

$$\boldsymbol{\tau}\cdot\boldsymbol{T}\boldsymbol{n} = \beta\boldsymbol{\tau}\cdot\boldsymbol{u}.$$

Here, $\boldsymbol{n}$ denotes the unit outward normal to the solid; $\boldsymbol{\tau}$ denotes $\boldsymbol{u}/|\boldsymbol{u}|$; $\boldsymbol{u}$ and $\boldsymbol{T}$ denote the velocity field and the stress tensor evaluated at the solid surface, respectively; and β, a constant, is often referred to as the slip coefficient. There are situations when contact lines are not present in which this boundary condition is recognized to be appropriate, the most notable being the case of rarefied gases, i.e. when the mean free path of the gas molecules becomes comparable with the characteristic lengthscale of the problem. A slip boundary condition has also been derived for systems consisting of non-dilute multi-component gases at standard temperature and pressure (Jackson 1977). In this latter case, it is of interest to note that using the no-slip boundary condition on the mass-averaged velocity, the velocity appearing in the Navier–Stokes equation, can lead to substantial error. In the context of the moving contact line, a derivation of β has been presented based upon an idealized model of a rough solid surface (Hocking 1976). Other slip boundary conditions, besides Navier's, have been proposed involving relationships between the shear stress and speed of the fluid at the solid surface (Huh & Mason 1977; Durbin 1988). These have been motivated by heuristic molecular models in which the strengths of the liquid–liquid and fluid–solid molecular bonds play a central role. Still another approach has been to explicitly prescribe the velocity of the fluid at the solid surface in such a way that the singularity at the moving contact line is removed, while preserving the no-slip condition away from the contact line (Dussan V. 1976).

There have also been investigations of the dynamics of the fluids in the immediate

vicinity of the moving contact line which do not presuppose that the fluids slip along the solid surface. Jansons (1986) assumes that the dynamics of the fluids within this small region are fundamentally unsteady owing to the microscopic roughness (on a continuum lengthscale) which is always present on the solid surface. He argues, based upon results from hydrodynamic analyses aimed at capturing the essence of various aspects of his idealization of the unsteady motion, that its impact on the dynamics of the fluid, as viewed from a much larger lengthscale, is equivalent to steady flow in the neighbourhood of the contact line with a slip boundary condition. However, the most fundamental attempts at exploring the physics of the fluids in the immediate vicinity of the moving contact line have been the molecular dynamics simulations by Koplik, Banavar & Willemsen (1988), and Thompson & Robbins (1989). Both studies follow the dynamics of approximately 1500 atoms, confined between two parallel walls separated by about 15 atomic spacings, in which the interactions between atoms are modelled with a modified Lennard–Jones potential. By altering the potential for interactions between like and unlike atoms, they are able to create a system consisting of two immiscible fluids and solid. They determine the velocity fields by dividing the confined region containing the atoms into bins, and by time averaging the instantaneous velocities of the atoms within each bin. Both studies obtain overall velocity fields in general agreement with solutions to the Navier–Stokes equation assuming the no-slip boundary condition (the former study simulates a Poiseuille-like flow, while the latter simulates a Couette-like flow), except within about two atomic spacings of the moving contact line, where the fluids slip along the solid surface, a region within which Thompson & Robbins find indications that the applicability of 'local hydrodynamic theory breaks down'. In spite of the latter, Thompson & Robbins find that the velocity field obtained from their molecular dynamics simulation agrees well with the solution of the Navier–Stokes equation assuming the fluid slips at the solid surface in the vicinity of the contact line, with slip length equalling about two atomic spacings.

It is of interest, as well as central to the nature of this investigation, to note that although the slip boundary conditions mentioned above are motivated by a diverse set of physical models, their effect is the same on the overall dynamics of the entire fluid body, i.e. the fluid in the *outer region*. This assumes, of course, the characteristic lengthscale of the outer region is large compared to that of the *inner region*, the region within which a significant amount of slip occurs. The lengthscale of this latter region will be referred to as the *slip length* L_s. As discussed in Ngan & Dussan V. (1989), the physics of the inner region (that is to say, choice of slip boundary condition, size of slip length, and dynamic behaviour of the 'actual' contact angle, θ), at small capillary and negligible Reynolds numbers, affects the dynamics of the fluids in the outer region only through the value of Ω, where

$$\Omega \equiv \theta + \frac{\mu U}{\sigma}\left\{\frac{2\sin\theta}{\theta - \cos\theta\sin\theta}\left[\ln\frac{a}{L_s}+1\right]+l_i(\theta)\right\}.$$

Here, a denotes the lengthscale of the outer region, μ denotes the viscosity of the liquid,† U denotes the speed of the contact line, σ denotes the surface tension, and $l_i(\theta)$ represents a function which depends on the form of the slip boundary conditions. This assertion is based upon analyses appearing in the literature valid to $O(\mu U/\sigma)$ as $\mu U/\sigma \to 0$, where $\mu U/\sigma$ is the capillary number Ca, holding L_s/a fixed,

† It is assumed that a liquid displaces a gas, or any other fluid, provided the viscosity ratio between the former and the latter is very large. The extension to a system consisting of two immiscible liquids having arbitrary viscosity ratio is straightforward.

with $L_s/a \ll 1$. Thus, knowledge of the dynamics of the fluids in the inner region determines the dynamics of the fluids in the outer region; however, the inverse is not true. That is to say, there is an infinity of combinations of Θ, L_s and l_t, be they velocity dependent or not, that give rise to the same value of Ω. This suggests that an explicit model of the dynamics of the fluids in the inner region may not be needed for determining the movement of fluids in the outer region. It may only be necessary to know the dynamic behaviour of Ω, which could possibly be determined from experiments on the macroscopic lengthscale.

Experimental investigations have been reported in the literature over the years quantifying the manner in which liquids spread on solid surfaces; however, none have been of the kind suggested at the end of the previous paragraph. Instead, the typical procedure for comparing experiment and theory focuses on the dependence of the apparent contact angle on the contact line speed. The *apparent contact angle* is not an actual angle, but rather represents an angle defined in terms of experimentally measurable quantities associated with the outer region, which in turn, depend very much on the shape of the body of fluids, and usually coincides with the actual contact angle under static conditions. For example, in the case of a capillary, a common definition of the apparent contact angle is $\cos^{-1} 2ha/(a^2+h^2)$, where a and h denote the radius of the capillary and the apex height, respectively. Most comparisons between theory and experiment follow the procedure of first assuming $\Theta = \Theta_a$ (Θ_a being the largest value of the contact angle under static conditions, measured from within the advancing fluid), and then choosing L_s to maximize agreement between the experimentally measured and theoretically predicted values of the apparent contact angle over a range of contact line speeds (Huh & Mason 1977; Lowndes 1980; Hocking & Rivers 1982; Cox 1986). In the light of the above discussion of Ω, it is evident that this procedure can at most determine the value of Ω over the range of contact-line speeds being investigated, but not the terms of which it is composed. Also, this procedure fails to address the more fundamental issue of whether or not an analysis which assumes a slip boundary condition accurately describes the dynamics of the fluids as seen from the macroscopic lengthscale (the outer region). This failure can be illustrated using the example of the capillary. Determining Ω at a particular speed based upon the apparent contact angle does not guarantee agreement between theory and experiment on the dynamics of the fluid within the entire outer region. It only assures that the location of the interface, in both theory and experiment, coincides at both the contact line and the apex, with no assurance of agreement along the remainder of the fluid interface in the outer region.

Ngan & Dussan V. (1989) present an alternative procedure for comparing theory and experiment, and for making use of the theory. They reasoned that the appropriateness of using a slip boundary condition to describe the dynamics of the fluids in the outer region can be determined by examining the overlap region, the domain common to both inner and outer regions. (This should not be confused with establishing that the fluids actually slip on the solid surface.) They argued that an examination of the shape of the fluid interface would suffice. If a slip boundary condition is appropriate, then the fluid interface obeys

$$\theta \sim \Omega + \frac{\mu U}{\sigma} \frac{2 \sin \Omega}{\Omega - \cos \Omega \sin \Omega} \ln \frac{r}{a}, \tag{1.1}$$

where a again denotes the lengthscale associated with the outer region. Here, the shape of the fluid interface is given in terms of the dependence of its local slope, θ,

relative to that of the solid surface, on the distance, r, from the moving contact line. Their objective was to measure θ at numerous values of r, and to see if a value of Ω could be found for which the data would agree with (1.1). Repeated comparisons over a range of contact line speeds would determine the dependence of Ω on U. They reasoned that if $\Omega(U)$ could be experimentally measured, then the usual assumptions in fluid mechanics (including the no-slip boundary condition), with the contact-angle boundary condition replaced by (1.1), would represent a well-posed problem, independent of whether or not fluid actually slips on solid surfaces.

Although the replacement of the contact-angle boundary condition by (1.1) may given rise to a well-posed problem, its general utility may be put into question due to the appearance of a in (1.1) and in the definition of Ω. This suggests that both $\Omega(U)$ and $\theta(r)$ depend upon the geometry of the device within which they are measured, which in turn would imply that $\Omega(U)$ could only be used to analyse the dynamics of fluids in systems whose geometry is identical to that of the measuring device. However, this is not the case. The a in both Ω and (1.1) cancel each other, as can be demonstrated by substituting the definition of Ω into (1.1), and retaining terms up to and including $O(\mu U/\sigma)$, as $\mu U/\sigma \to 0$. Motivated by the desire to make this transparent, Ngan & Dussan V. introduced the parameter θ_R, defined to be the value of θ at $r = R$, R representing a specified distance from the contact line, located within the overlap region. Thus,

$$\theta \sim \theta_R + \frac{\mu U}{\sigma} \frac{2 \sin \theta_R}{\theta_R - \cos \theta_R \sin \theta_R} \ln \frac{r}{R}, \tag{1.2}$$

where

$$\theta_R = \theta + \frac{\mu U}{\sigma} \left\{ \frac{2 \sin \theta}{\theta - \cos \theta \sin \theta} \left[\ln \frac{R}{L_s} + 1 \right] + l_t(\theta) \right\}.$$

Unlike Ω, θ_R is independent of the geometry of the outer region, i.e. it represents a material property of the system.

Unfortunately, Ngan & Dussan V. were unable to directly measure the slope of the fluid interface, so they developed a procedure by which measurements of the apex height for oil displacing air through a set of narrow slots could be used to determine $\theta(r)$ near the contact line. Note that their method differs significantly from that used by others described above. Ngan & Dussan V. use multiple measurements taken at the *same* contact line speed, but with slots having different gap widths (different values of the lengthscale of the outer region), to deduce $\theta(r)$ near the contact line, while the typical procedure uses many measurements, each taken at different contact line speeds to determine a single value for L_s. Their results showed good agreement with (1.2); however, systematic deviations were found between their experimentally measured and theoretically determined values of the apex height.

The objective of this study is the same as Ngan & Dussan V. (1989). The heart of this investigation consists of comparing experimental measurements to a theoretical expression of the shape of the fluid interface near the contact line. Instead of using (1.2), we use the shape arising in the intermediate region, the additional region in the three-region approach of Hocking & Rivers (1982) and Cox (1986). This region is located between the inner and outer regions, having a dimensionless length of $(\mu U/\sigma) \ln r/a$, the expansions for all three regions being defined as $\mu U/\sigma \to 0$, holding $(\mu/U/\sigma) \ln L_s/a$ fixed. Note that $(\mu U/\sigma) \ln L_s/a \sim 1$ in the three-region expansion, while $(\mu U/\sigma) \ln L_s/a \to 0$ in the two-region one. Thus, the motivation for including the intermediate region is that it accounts for the viscous effects on the shape of the fluid interface at $O(1)$ as $\mu U/\sigma \to 0$ more accurately than the two-region solution does, at

$O(\mu U/\sigma)$ as $\mu U/\sigma \to 0$. (W. Boender & A. K. Chesters (1986, private communication) have shown, for the case of flow through a capillary, excellent agreement within the intermediate region between the lowest-order three-region solution and the numerical solution of Lowndes (1980), for $\mu U/\sigma < 8 \times 10^{-2}$.) In §2, experiments are presented consisting of immersing a glass tube into a bath of silicone oil, which enable direct measurements to be made of $\theta(r)$ near the contact line, an advantage over the experiments of Ngan & Dussan V. In §3, the explicit form of $\theta(r)$ is presented which we use to compare theory with experimental measurements. In this section alternative expressions are also presented of both Ω and (1.2), because these (and (1.1)) only apply when two regions are sufficient. We end with a discussion and conclusions in §4.

2. Experiments

2.1. *Procedure*

The experiments consisted of immersing a glass tube with an outer diameter of 2.54 cm, denoted by $2R_T$, at a constant speed U, and at an angle α relative to the horizontal, into a bath of liquid in a direction parallel to its axis; refer to figure 1. The outer diameter of the tube was chosen so that the shape of the fluid interface in the region of observation differed slightly from that formed by an infinite flat plate (see Appendix A). These experiments have several obvious advantages over others. (i) They need not be restricted to transparent materials, as is the case for the displacement of fluids through a capillary or between two parallel plates. (ii) Unlike the inconvenience associated with a spreading drop, measurements can be made over a range of constant specified contact-line speeds with, in principle, no restrictions placed on the contact angle. (iii) The lengthscale of the outer region, denoted by a, is $(\sigma/\rho g)^{\frac{1}{2}}$, often referred to as the capillary length, represents the largest lengthscale achievable in an outer region dominated by surface tension. This enables measurements of the shape of the fluid interface to be made at the smallest possible value of r/a for a given distance, r, from the contact line. (iv) The apparatus can easily be modified to accommodate two immiscible liquids, although we have only investigated the case of a liquid displacing air. (v) The shape of the interface close to the moving contact line can be accurately measured as a continuous function of position.

The choice of materials, and their preparation are as follows. Silicone oil (Dow Corning 200) was used because its low surface tension minimizes the tendency of the fluid interface to attract contaminants. Its viscosity, density and surface tension were 11.8 P, 0.974 g/cm^3, and 21.8 dyn/cm, respectively, throughout the course of the experiments. These values were obtained by using a Paar DMA digital density meter, a Cannon-Fenske viscometer and a Du Nouy ring, respectively, all representing standard laboratory instruments. The container holding the silicone oil was a 400 cm^3 Teflon beaker. Initially, it was cleaned with a mild soap solution, then rinsed thoroughly with deionized water, and allowed to soak for two days in silicone oil. The Teflon beaker was then refilled with fresh silicone oil for the duration of the experiments, always kept completely full to minimize contamination. The glass tube was cleaned by the following procedure. It was initially soaked for 20 minutes in chromic/sulphuric acid (consisting of 15 g $K_2Cr_2O_7$, 25 ml H_2O, and 500 ml H_2SO_4, rinsed thoroughly with deionized water, soaked for an additional 20 minutes in a water solution consisting of 20% by volume HCl, and again rinsed thoroughly with deionized water. A jet of nitrogen gas was then used to blow off the water from the

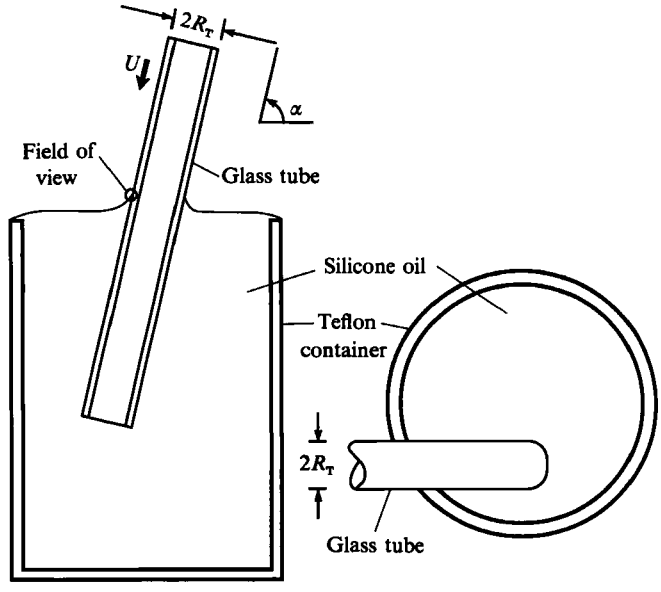

FIGURE 1. A sketch of the glass tube being immersed into the teflon beaker filled with silicone oil. Two different views are presented: (*a*) the side view; and (*b*) the plan view. The glass tube is immersed off-centre into the beaker, as shown in (*b*). The field of view of the video camera is indicated in (*a*).

tube. If the water was not pushed off the surface as a continuous sheet, then the cleaning procedure was repeated.

The glass tube was attached to a DC motor-driven translation stage (Newport Corporation Model 860 Series), which immersed the tube into the bath of oil at a relatively constant speed. Two motors with different gearing were used, one for the slowest speed, and another for the remaining speeds.

The arrangement of the different components of the experimental apparatus is presented in figure 2. The glass tube, partially submerged in the silicone oil contained within the Teflon beaker, is located between a tungsten light source and a high-resolution video camera (Ikagami Model 510) fitted with a Bausch & Lomb Monozoom 7 long working distance microscope. The view of the fluid interface is from the perspective of figure 1 (*a*), and is limited to the encircled region containing the moving contact line. With this illumination, both the tube and fluid interface appear as a shadow. The image is sent to a thermal printer, a video cassette recorder, and a television monitor. The image from the printer has a magnification of 300 times. Measurements are read off a copy made with a Cannon Laser Copier of the thermal print, which further magnified the image an additional four times, giving a total magnification of 1200 times.

Special care was taken to align the camera, glass tube, and light source so that the image was representative of the interface shape in a plane containing the rod axis. Using an optical rotation stage, the glass tube was pivoted to achieve the desired angle of immersion, α. Further adjustments were made to the position of the tube to ensure that its pivot plane and the fluid interface were perpendicular, and that the motor moved the tube in a direction parallel to its axis. The microscope and the beam produced by the tungsten light source were placed so that their axes coincided,

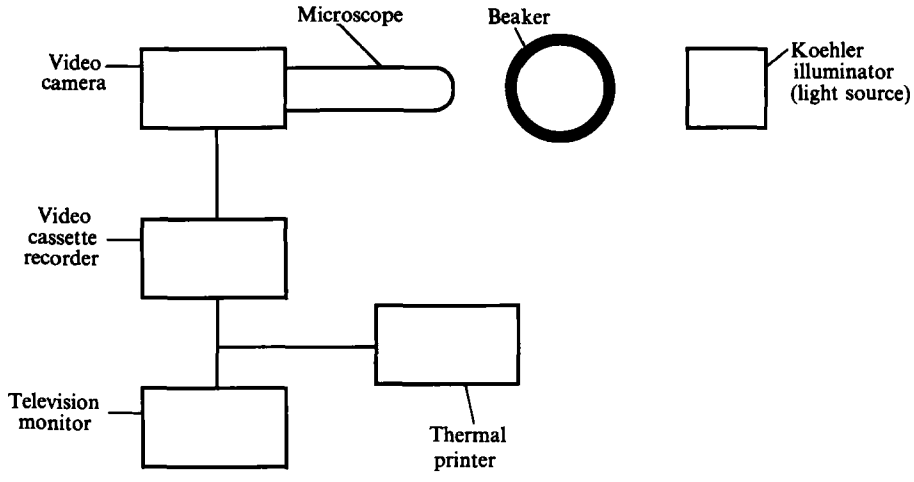

FIGURE 2. A schematic of the apparatus.

intersecting the pivot plane of the tube at right angles. The vertical movement of the fluid interface was minimized during the immersion of the tube into the silicone oil by completely filling the Teflon beaker until the oil spilled over the edge. The angle α was measured by superimposing two prints: one of a rather thin wire attached to a plumb bob; and the other of just the glass tube in the same position as when it was immersed into the oil.

A typical picture from the thermal printer appears in figure 3. Note that both the surface of the glass tube and the fluid interface generate a series of bands resulting from the diffraction of light. If the curvature is constant over that part of the surface diffracting the light, then the bands are parallel to the edge of the object, with the intensity of the bands being proportional to the magnitude of the curvature parallel to the incident light beam (van de Halst 1979). In the present case, the glass tube has a constant curvature, but not the fluid interface. Nevertheless it is assumed that the bands produced by the fluid interface are parallel to the edge of the fluid interface. This is supported by the observation that the variation in spacing between the bands is insignificant. The shape of the interface was quantified by measuring the slope of the boundary of the large darkened area relative to the surface of the glass tube, θ, with a protractor at numerous positions along the boundary. Unfortunately, an interference pattern can be detected near the contact line where the diffraction patterns meet resulting in a 'kink'. This places a limitation on the closest distance to the contact line for which θ can be measured with the present technique, that is, approximately 25 μm. This distance reduces to about 18 μm at our slower speeds, a consequence of the decrease in slope of the fluid interface when the contact line speed is decreased.

Approximately fifteen lines were drawn parallel to the solid surface on the enlarged copy of the image at positions distributed along the fluid interface. The fluid interface was interpreted as a curve connecting picture elements of fixed grey level. The slope of the interface, reported at a given position, represents the average of five to ten independent readings made with a protractor. Measurements were made at positions along the interface varying in distance from the contact line by between approximately 25 to 250 μm the latter representing $0.165a$.

The image obtained from the thermal printer contained a measurable amount of systematic distortion, whose magnitude varied with position within the image. The

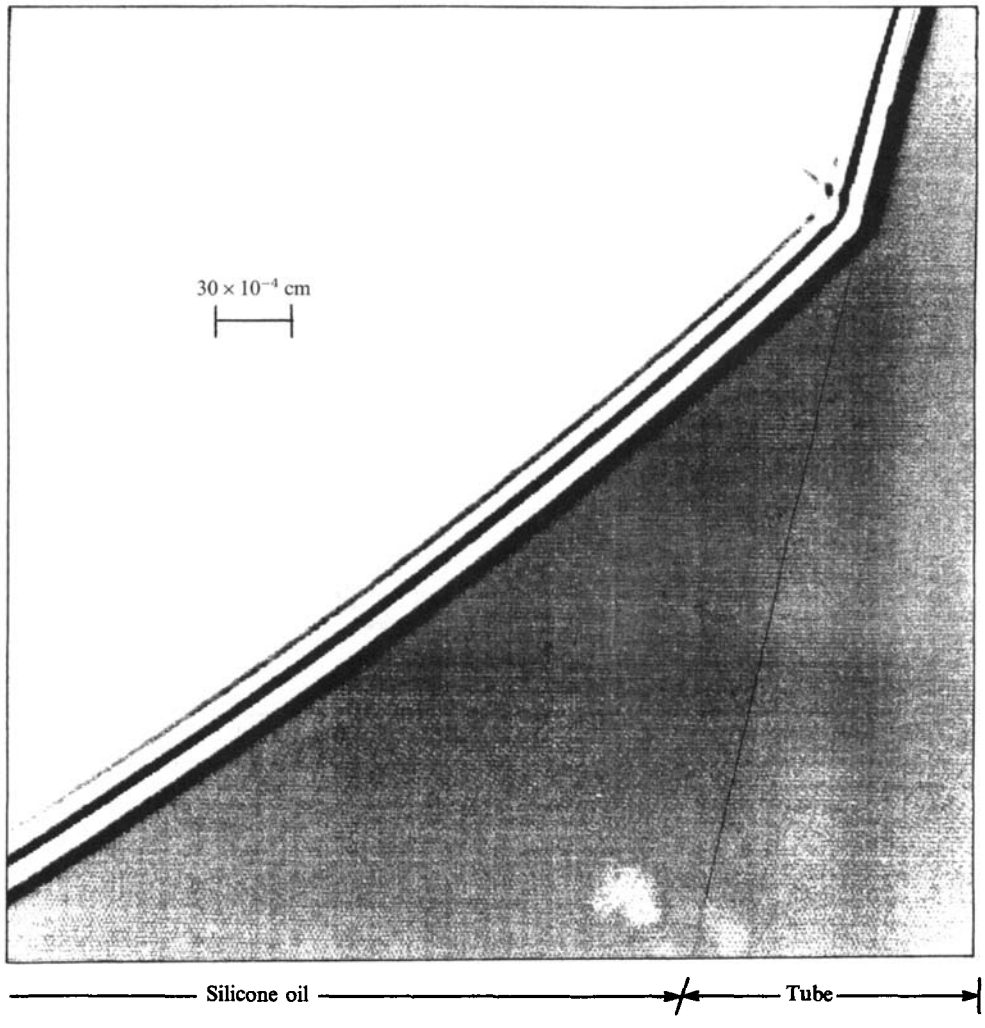

FIGURE 3. A typical thermal print of the fluid interface.

distortion was quantified by analysing a number of images of a straight edge located in the field of view close to the images of the fluid interface of interest, the prints of the images of the straight edge and fluid interface having been taken at different times. It should be noted that the images of the fluid interface do not differ much from that of a straight line. Each straight-edge image was characterized by measuring its slope relative to the direction of the tangent vector at its end closest to the centre of the print, at evenly spaced points along its length. The extent to which the values of these slopes differ from zero is a quantitative indication of the distortion. The distortion of the image of each fluid interface was removed by subtracting from the measured slopes along its length the slopes corresponding to the straight-edge image. The slopes of the straight-edge image, at these specific positions, were obtained from an evaluation of a second-order polynomial, derived from a least-squares fit of the data measured from the image of the straight edge. The final step of enlarging the thermal print with the Cannon Laser Copier did not introduce any detectable distortion.

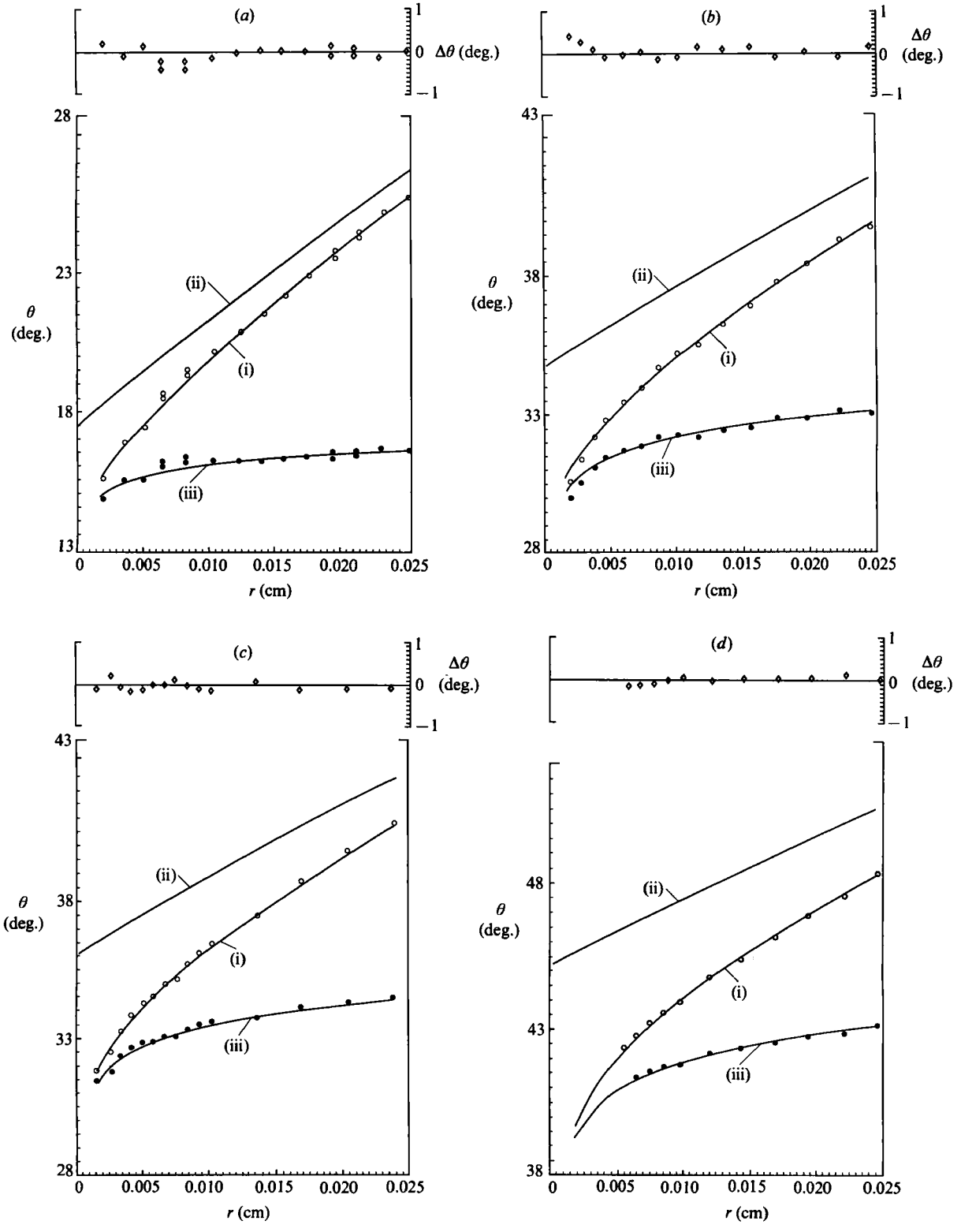

FIGURE 4 (*a–d*). For caption see facing page.

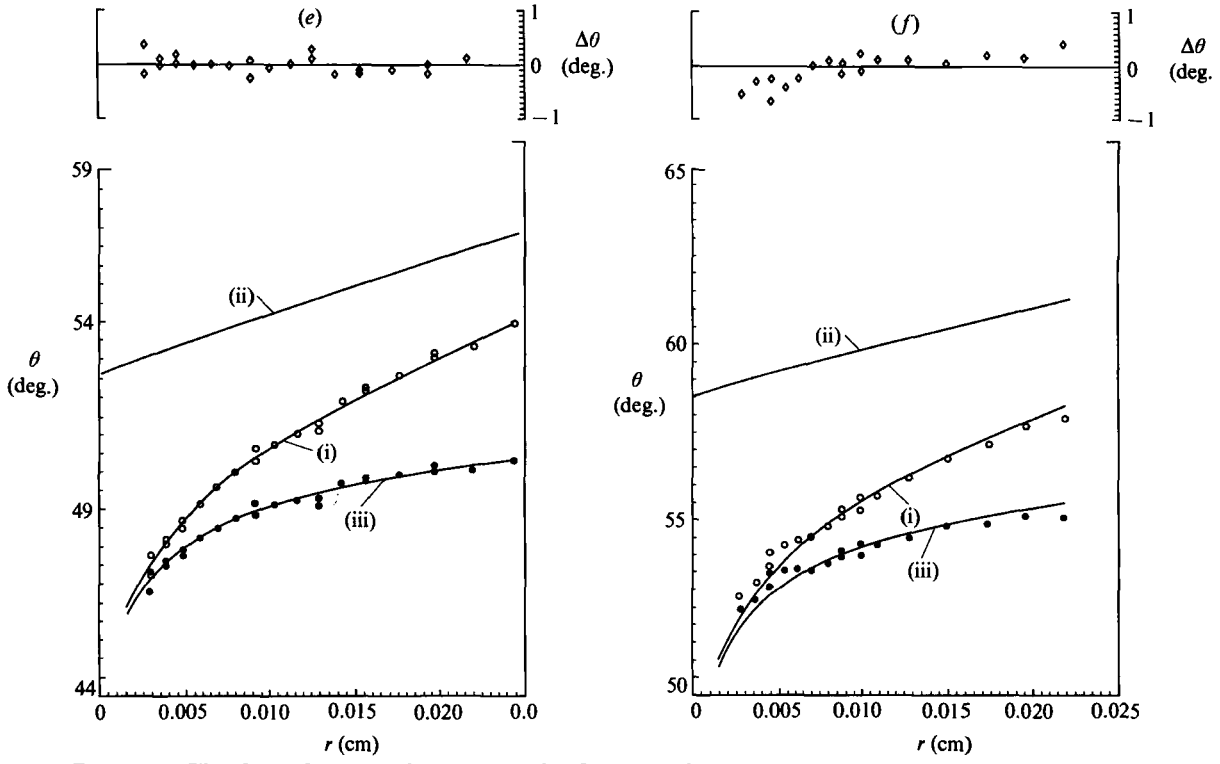

FIGURE 4. The dependence of the slope of the fluid interface, θ, and the difference between the theoretically predicted and experimentally measured slopes, $\Delta\theta$, on the radial distance from the contact line, r: (*a*) $Ca = 2.76 \times 10^{-4}$; (*b*) $Ca = 1.86 \times 10^{-3}$, (*c*) $Ca = 2.08 \times 10^{-3}$; (*d*) $Ca = 4.13 \times 10^{-3}$; (*e*) $Ca = 6.47 \times 10^{-3}$; (*f*) $Ca = 8.74 \times 10^{-3}$. The experimentally measured values of θ are denoted by ○. The curves (i), (ii) and (iii) in each graph denote the composite solution, (3.9), the outer solution, (3.3), and the intermediate solution, $(3.9)-(3.3)+\omega_0$, respectively. The symbol ● denotes $(3.3)-\omega_0$ subtracted from the data.

An important aspect of the experimental procedure consisted of choosing thermal prints for analysis. Several prints of seemingly the same event may differ owing to small fluctuations in the motor speed, or disturbances resulting from imperfections on the surface of the rod. Two prints were regarded as recording *equivalent* events if upon superposition of the prints the shapes of the interface coincided, and the relative orientation of the glass tube agreed to within 0.5°. Thus, a series of at least six prints were taken of any given event. A print was accepted for analysis only if it belonged to a set of two or more equivalent prints.

The principal experiments consisted of immersing the glass tube into the bath of silicone oil at an angle α equal to 78.5°, and at six different speeds corresponding to capillary numbers of 2.76×10^{-4}, 1.86×10^{-3}, 2.08×10^{-3}, 4.13×10^{-3}, 6.47×10^{-3} and 8.74×10^{-3}; refer to figure 4(*a–f*), each graph in the figure representing measurements from an individual print. There is no significance to the value of α chosen, other than convenience. However, small capillary numbers were desired because the objective of these experiments was to compare the shape of the fluid interface with that predicted by theory, valid in the limit as $\mu U/\sigma \to 0$.

2.2. *Error analysis*

There are various errors associated with our measurements, and with the experiments themselves. A significant portion arose from the distortion of the image, and the methods used for measuring $\theta(r)$ and α. We begin by addressing these issues. We end with a brief discussion of the errors introduced by the fluctuations in the speed of the motor as the tube is immersed into the bath of silicone oil, by cleaning, and by the measurements of the material properties of the silicone oil.

The distortion of the image could have arisen from many factors. It was quantified by examining the images of a straight edge located at positions close to those of the fluid interfaces in figure 4 (refer to Appendix B for details). The measurements of $\theta(r)$ using the protractor were surprisingly reproducible, the limiting factor being the size of the variation of its curvature. We found that the more rapid the variation in the curvature, the more difficult the measurement. The standard deviation associated with ten repeated measurements of θ at a point on the fluid interface was approximately 0.25° near the contact line, decreasing to 0.15° at distances beyond about 100 μm. At points on the images of the straight edge, the standard deviation was about 0.15° throughout. The accuracy of θ also depended on being able to draw lines through points on the images of the fluid interface and the straight edge that were parallel to the surface of the tube. While there was very little error associated with drawing the lines parallel to each other, our method could give rise to approximately a $\pm 0.5°$ deviation in slope between the parallel lines and the surface of the tube. Such an error manifests itself in each graph of θ in figure 4 as a constant shift of all the data points in the direction parallel to the θ-axis. An error of $\pm 0.1°$, accounting for the residual distortion, has been combined with the random errors in measuring θ to give a total error of $\pm 0.27°$ close to the contact line, and $\pm 0.18°$ beyond 100 μm. These values ignore the above-discussed uncertainty of $\pm 0.5°$, the justification of which appears in §3.2. The error in α was also estimated to be $\pm 0.5°$, primarily resulting from the distortion of the images (see Appendix B).

When the experiments were performed at the slowest speed, it was evident that the tube was not being immersed into the oil at a constant speed. Upon further investigation, we found the slow motor had a reproducible periodic fluctuation of $\pm 18\%$, probably produced by poorly manufactured gears. No such problem was noticed with our faster motor, which was used in the bulk of our experiments.

Our material system did not change during the course of our experiments, at least to within our experimental error. This can be assessed by the degree to which the material properties of the system, including the properties of the solid surface, remain constant. The density, viscosity and surface tension were measured at the beginning and conclusion of the investigation. We found that they varied in value by less than 1%. The reproducibility of the solid surface can be assessed by repeating experiments after cleaning the glass tube. Upon repeating a limited number of experiments, we found agreement to about $\pm 0.5°$. This is comparable with the agreement between the analysis of two thermal prints of the same experiment.

3. Theory and results

3.1. *Theory*

The experimental measurements are compared to theory correct to $O(1)$ as $\mu U/\sigma \to 0$, holding $(\mu U/\sigma) \ln L_s/a$ fixed, obtained from a three-region expansion characterized by dimensionless lengths r/L_s, $(\mu U/\sigma) \ln r/a$, and r/a, where a denotes the capillary

length, $(\sigma/\rho g)^{\frac{1}{2}}$. Throughout this section it is understood that $(\mu U/\sigma)\ln L_s/a$ is held fixed whenever $\mu U/\sigma \to 0$.

The shape of the fluid interface within each of the three regions is as follows. In the intermediate region, as pointed out by Hocking & Rivers and Cox, the shape of the fluid interface, correct to $O(\mu U/\sigma)$ as $\mu U/\sigma \to 0$, is given by

$$\theta \sim g^{-1}(d_0 + d_1(\mu U/\sigma) + (\mu U/\sigma)\ln r/a), \tag{3.1}$$

where d_0 and d_1 are constants to be determined by matching the intermediate to the inner solution, g^{-1} denotes the inverse function of g, that is to say, $x \equiv g^{-1}(g(x))$, and the function g is defined by

$$g(x) \equiv \int_0^x \frac{\rho - \sin\rho\cos\rho}{2\sin\rho}\,\mathrm{d}\rho. \tag{3.2}$$

Since our main concern is with the shape of the fluid interface in the intermediate and outer regions, it suffices to present only the asymptotic form of $\theta(r)$ in the inner region, valid as $r/L_s \to \infty$,

$$\theta \sim \Theta + \frac{\mu U}{\sigma}\left\{\frac{2\sin\Theta}{\Theta - \cos\Theta\sin\Theta}\left[\ln\frac{r}{L_s} + 1\right] + l_i(\Theta)\right\}.$$

This represents a general form which has arisen when a slip boundary condition has been assumed, also correct to $O(\mu U/\sigma)$ as $\mu U/\sigma \to 0$ (refer to Ngan & Dussan V. for further discussion). The shape of the fluid interface in the outer region, correct to $O(1)$ as $\mu U/\sigma \to 0$, denoted by f_0, retains the same form as under static conditions, the only difference being that the term representing the static contact angle, which shall be denoted as ω_0, is now regarded as a constant to be determined by matching the outer to the intermediate solution, where

$$\theta \sim f_0(r/a; \omega_0, R_T/a, \alpha), \tag{3.3}$$

its explicit form being the right-hand side of (A 3), with ω_0 replacing Θ.

Matching the intermediate to the inner solution gives

$$d_0 = g(\Theta) + (\mu U/\sigma)\ln a/L_s, \tag{3.4}$$

$$d_1 = 1 + l_i(\Theta)\{\Theta - \sin\Theta\cos\Theta\}/2\sin\Theta. \tag{3.5}$$

Substituting (3.4) and (3.5) into (3.1) gives an expression for the shape of the interface in the intermediate region of the form

$$\theta \sim g^{-1}(g(\Theta) + (\mu U/\sigma)\ln r/L_s + \mu U/\sigma(1 + l_i(\Theta)\{\Theta - \sin\Theta\cos\Theta\}/2\sin\Theta)),$$

correct to $O(Ca)$, as $Ca \to 0$, matching the outer to the inner solution gives

$$\omega_0 = g^{-1}(d_0). \tag{3.6}$$

Substituting (3.4) into (3.6) gives

$$\omega_0 = g^{-1}(g(\Theta) + (\mu U/\sigma)\ln a/L_s). \tag{3.7}$$

Comparisons are made between the experimental measurements of θ and a composite solution, a little beyond the region where the intermediate and outer solutions overlap. The composite solution is obtained by combining (3.1) and (3.3) to give

$$\theta = g^{-1}(d_0 + (\mu U/\sigma)\ln r/a) + f_0(r/a; \omega_0, R_T/a, \alpha) - \omega_0, \tag{3.8}$$

where d_0 and ω_0 are given by (3.4) and (3.7), respectively, the above expression being correct to $O(1)$ as $\mu U/\sigma \to 0$. Note that (3.8) is equivalent to

$$\theta = g^{-1}(g(\omega_0) + (\mu U/\sigma)\ln r/a) + f_0(r/a; \omega_0, R_T/a, \alpha) - \omega_0. \tag{3.9}$$

This is the expression which we use in our comparisons between theory and experiments.

Although ω_0 (referred to as the *apparent* contact angle by Hocking & Rivers 1982 and Cox 1986 because of its influence on the shape of the fluid interface in the outer region) is a convenient parameter to use when comparing theory and experiment, it is not an appropriate parameter to use in (3.1) when (3.1) replaces the contact-angle boundary condition. This is a consequence of the dependence of ω_0 on a, the capillary length (refer to (3.7)) falsely suggesting that $\theta(r)$, in the intermediate region, also depends on the lengthscale (and thus, the geometry) of the outer region. (This impression may result from substituting (3.6) into (3.1), and ignoring the term containing d_1 because ω_0 has been determined using (3.9), an equation correct to $O(1)$.) For this reason, we follow Ngan & Dussan V. by parameterizing (3.1) in terms of Θ_R (refer to §1), with the alteration that R now denotes a specific location in the intermediate region. (From a practical point of view, R may be regarded as representing a position within the intermediate region when the solution valid in the outer region has an ignorable effect on the composite solution, for example, when $|f_0(R/a; \omega_0, R_T/a, \alpha) - \omega_0|$ is a negligible quantity, for all values of α. Thus, either (3.1) or (3.9) can be used.) Evaluating (3.1) at R, gives

$$\Theta_R \sim g^{-1}(d_0 + d_1 \mu U/\sigma + (\mu U/\sigma)\ln R/a), \tag{3.10}$$

and using (3.10) to eliminate $d_0 + d_1 \mu U/\sigma$ from (3.1), gives

$$\theta \sim g^{-1}(g(\Theta_R) + (\mu U/\sigma)\ln r/R). \tag{3.11}$$

The fact that Θ_R depends upon the physics of the inner region, and not on a follows from (3.10), (3.4) and (3.5).

Note that the comments in the introduction regarding Ω remain valid after extending its definition to

$$\Omega \equiv g^{-1}(g(\Theta) + (\mu U/\sigma)\ln a/L_s + \mu U/\sigma(1 + l_i(\Theta)\{\Theta - \sin\Theta\cos\Theta\}/2\sin\Theta)),$$

It is evident that Ω may be regarded as an *apparent contact angle*, correct to $O(Ca)$ as $Ca \to 0$. Retaining only $O(1)$ terms gives the same expression as ω_0.

3.2. *Results*

The objective is to compare, at a given contact line speed U, the experimentally measured dependence of θ on r to the theoretically predicted expressions presented above. Since independent knowledge of d_0, i.e. ω_0, is unavailable, our procedure for making this comparison must incorporate the determination of its value.

As mentioned in §2, experimental measurements were made at distances from the contact line varying between about 20 and 250 μm. This corresponds to values of r/a ranging from 0.013 to 0.165, a being equal to 1511 μm. Since this corresponds, at least in part, to the outer region, the composite solution for $\theta(r)$ is regarded as correct to $O(1)$ as $\mu U/\sigma \to 0$.

The comparisons were made using (3.9). There is only one unknown in this equation: the value of the parameter ω_0. For each set of data, ω_0 was chosen so that the theoretical function $\theta(r)$ best fits, in the least-square sense, the data over its entire range, refer to the solid line labelled (i) passing through the data in the graphs of

U (cm/s)	Ca	ω_0 (deg)	θ_R (deg)
5.12×10^{-4}	2.76×10^{-4}	17.58	14.95
3.44×10^{-3}	1.86×10^{-3}	34.78	29.95
3.86×10^{-3}	2.08×10^{-3}	36.12	31.12
7.60×10^{-3}	4.12×10^{-3}	45.27	38.74
1.20×10^{-2}	6.47×10^{-3}	53.28	45.79
1.61×10^{-2}	8.74×10^{-3}	58.58	50.10

TABLE 1. Silicone oil displacing air from the surface of a glass tube at speed U. The values of θ_R are based upon $R = 10^{-3}$ cm.

figure 4. The differences between the theory and the data, denoted by $\Delta\theta$, are plotted across the upper portion of each graph in the figure. Curve (ii) in this figure represents the solution in the outer region, i.e. (3.3), the portion of the solution responding to the influence of gravity. While curve (iii) represents the solution in the intermediate region, i.e. $(3.9)-(3.3)+\omega_0$, the portion of the solution being deformed only by the viscous forces. The solid circles neighbouring (iii) were obtained by subtracting $(3.3)-\omega_0$ from the data. The values of ω_0 are presented in table 1.

It should be noted that adding a constant (having absolute value less than 0.5°) to all the experimental data in any one of the graphs in figure 4 results in a new value of ω_0, within $\pm0.5°$ of its original value, with no perceptible alteration to the appearance in the systematic deviation between theory and experiment from that originally calculated (refer to the upper portion of the appropriate graph). This is the reason for not including the two errors of approximately $\pm0.5°$ each, referred to at the end of the second paragraph of §2.2, in the estimated error of our measurements of θ. Simply put, our attention is focused on the degree of agreement (or lack there of) between theory and experiment with respect to the viscous bending of the fluid interface, not the precision to which the value of ω_0 can be determined. A calculation of the latter would require the inclusion of the two errors referred to above.

4. Discussion and conclusions

The objective of this study was to measure the viscous bending of a liquid–air interface very close to a moving contact line, and to compare it to solutions of the Navier–Stokes equation (assuming the usual hydrodynamic model, including the no-slip boundary condition). Our motivation was to determine the validity of a general procedure presented by Ngan & Dussan V. for obtaining solutions to problems containing moving contact lines, which bypasses the necessity of explicitly identifying the physics governing the dynamics of the fluids in the immediate vicinity of the moving contact line. The crux of this procedure consists of replacing the contact-angle boundary condition by the asymptotic form of the slope of the fluid interface in the intermediate region, (3.1) (or equivalently, (3.11)), the constants in this expression having been empirically determined.

We wanted to measure the slope of the fluid interface, θ, as close as possible to the moving contact line so that it would be dominated by its asymptotic form as $r\to0$. This would have enabled us to use (3.1), an expression correct to $O(\mu U/\sigma)$ as $\mu U/\sigma\to0$. Instead, our measurements were in the outer region, which necessitated the use of (3.9), the composite solution, an expression known with less accuracy, being correct to $O(1)$ as $\mu U/\sigma\to0$. Nevertheless, we still wanted the measurements of θ to be made as close to the contact line as possible, so that the behaviour of the fluid

interface in the neighbourhood of the contact line would dominate our measurements. The heart of the investigation consisted of measuring θ near the moving contact line located on a glass tube being immersed at a constant speed into a bath of silicone oil, and comparing these measurements to (3.9). Measurements were taken at six different contact-line speeds. The comparisons between theory and experiment appear in figure 4, and the values of ω_0 (the matching constant) at each contact line speed appear in table 1. Since the measurements lie within the estimated error, with little or no systematic deviations (except at the highest contact-line speed), we conclude that our data support using (3.1) as a boundary condition for the shape of the fluid interface in the outer region.

As discussed in the second to last paragraph in §3.1, the matching constant, ω_0, depends upon the lengthscale of the outer region. Thus, $\omega_0(U)$ is not a material property of the system, i.e. $\omega_0(U)$ measured in one geometry of the outer region does not apply to the same materials in a different geometry. For this reason, the parameter Θ_R, a property strictly of the materials, was introduced. With this parameterization, (3.11) replaces (3.1) as the boundary condition at the contact line. The dependence of Θ_R on U, for $R = 10^{-3}$ cm (10 μm), corresponding to the six contact-line speeds of our experiments, is given in table 1, where Θ_R is obtained by evaluating (3.9) at $r = R$†. If our images had allowed measurements of θ at positions closer to the contact line, then we would have been able to directly measure Θ_R, and the experimental data would have been compared to a theory with no free parameters.

What does the conclusion on the direct measurement of Θ_R imply about the physics governing the dynamics of the fluid in the inner region? As stated in the introduction, it has been established that (3.1) is consistent with a wide variety of boundary conditions which permit the fluid to slip at the solid surface. However, (3.1) might also be consistent with an even larger class of physical models of the inner region. For example, Jansons' (1986) model consisting of an inherently unsteady inner region can be viewed from this perspective. This is an area which may deserve further research.

It is appropriate to state that these results share a weakness common to many studies based on an asymptotic analysis, a lack of knowledge of the magnitude of the expansion parameters which should not be exceeded for the solution to have the desired degree of accuracy. In this case, it would be of interest to know if the systematic deviation between experiment and theory evident at $\mu U/\sigma = 8.74 \times 10^{-3}$ is a consequence of an inadequacy in the composite solution, (3.9), resulting from using too large a value of $\mu U/\sigma$.

† Even though two quantities appear in this parameterization, it would not be proper to regard them as independent. It is easily seen that there exists a family $\{(R, \Theta_R)\}$ which satisfies (3.1) for a given value of ω_0; however, once R is specified, then Θ_R is unique. A criterion for choosing R could be

$$e = |f_0(R/a; \omega_0, R_T/a, \alpha) - \omega_0| \quad \text{for all values of } \alpha,$$

where e denotes the uncertainty in the measurement of θ. This implies that the contribution to the error in Θ_R arising from the residual influence of the geometry of the outer region on the composite solution, (3.9), has the same magnitude as the experimental error in θ. In the present experiment, e equals 0.27° so that the above criterion implies an approximate value of R of 10μ (refer to curve (ii) in figure 4).

Appendix A

There were two reasons why the meniscus formed outside the tube differed from that of a flat plate of infinite extent: (i) the tube had a finite, though large, radius, R_T, compared to the capillary length, a; and (ii) the axis of the tube was not parallel to the direction of gravity, intersecting the undisturbed fluid interface at an angle of 78.5°, as opposed to 90°, creating a meniscus varying in shape around the outside of the tube. Note that both of these effects were small, with the first dominating the second because of the relative smallness in size of $\frac{1}{2}\pi-\alpha$ (the second effect disappearing as $R_T/a\to\infty$, but the first remaining even if the tube was perfectly vertical). Thus, only the lowest-order effect resulting from (i) was calculated, equivalent to a static meniscus surrounding a vertical tube having a large radius.

With this understanding, the equation governing the shape of the meniscus is given by

$$\frac{\mathrm{d}^2h/\mathrm{d}r_c^2}{\{1+(\mathrm{d}h/\mathrm{d}r_c)^2\}^{\frac{3}{2}}}+\frac{\mathrm{d}h/\mathrm{d}r_c}{r_c\{1+(\mathrm{d}h/\mathrm{d}r_c)^2\}^{\frac{1}{2}}}=h,$$

subject to the boundary conditions

$$\mathrm{d}h/\mathrm{d}r_c=\tan(\Theta-\tfrac{1}{2}\pi)\quad\text{at}\quad r_c=R_T/a,$$
$$h\to 0\quad\text{as}\quad r_c\to\infty,$$

where $\{(r_c,h(r_c))\,|\,R_T/a<r_c<\infty\}$ represents the location of the meniscus using a cylindrical coordinate system, whose origin is on the axis of the tube at the same height as the undisturbed liquid–air interface far from the tube, with the z-axis pointing in the upward direction, and r_c and h are made dimensionless using a. The contact angle Θ is measured with respect to the vertical taken from within the liquid.

Local solutions near $(R_T/a, h(R_T/a))$ were obtained for the first two terms of an asymptotic expansion, valid in the limit as $R_T/a\to\infty$, of the form

$$h\sim h_0(x;\Theta)+\frac{a}{R_T}h_1(x;\Theta)+\ldots,$$

where

$$h_1\sim d_0+d_1x^2+d_3x^3+\ldots,$$

and x denotes r_c-R_T/a, the term h_0 corresponding to the shape of a meniscus adjacent to a flat plate.

The exact solution for h_0 is well known, given parametrically by

$$h_0=2\sin(\tfrac{1}{2}(\tfrac{1}{2}\pi-\theta)),$$
$$x=-2\cos(\tfrac{1}{2}(\tfrac{1}{2}\pi-\theta))-\ln\tan(\tfrac{1}{4}(\tfrac{1}{2}\pi-\theta))+2\cos(\tfrac{1}{2}(\tfrac{1}{2}\pi-\Theta))+\ln\tan(\tfrac{1}{4}(\tfrac{1}{2}\pi-\Theta)),$$

and it is straightforward to show that

$$\theta\sim\Theta+2r\sin(\tfrac{1}{2}(\tfrac{1}{2}\pi-\Theta))-\tfrac{1}{2}r^2\sin(\tfrac{1}{2}\pi-\Theta)$$
$$+\frac{a}{R_T}\{r(d_0+\sin(\tfrac{1}{2}\pi-\Theta))-r^2\sin(\tfrac{1}{2}(\tfrac{1}{2}\pi-\Theta))\cos(\tfrac{1}{2}\pi-\Theta)\},\quad\text{(A 1)}$$

where r and θ retain the same meaning as in §1. An evaluation of d_0 requires knowledge of the solution for h_1 over the entire interval $x\in[0,\infty)$. Huh & Scriven (1969) have verified that the following formula of Ferguson is correct to within 1% for $R_T/a\geqslant 1$:

$$\tfrac{1}{2}h^2|_{x=0}-1-\frac{4}{3}\frac{a}{R_T}[(1-\tfrac{1}{4}h^2|_{x=0})^{\frac{3}{2}}-1]+\sin\Theta=0.$$

This implies
$$d_0 = \frac{2}{3\sin\left(\frac{1}{2}(\frac{1}{2}\pi - \Theta)\right)}\left[\cos^3\left(\tfrac{1}{2}(\tfrac{1}{2}\pi - \Theta)\right) - 1\right]. \tag{A 2}$$

Substituting (A 2) into (A 1), replacing $\frac{1}{2}\pi - \Theta$ by $\alpha - \Theta$ (implying $\frac{1}{2}\pi - (\alpha - \Theta)$ replaces Θ), and replacing θ by $\frac{1}{2}\pi - (\alpha - \theta)$ gives the formula used in this study:

$$\theta = \Theta + \left[2\sin\left(\frac{\alpha-\Theta}{2}\right) + \frac{a}{R_T}\left\{\frac{2}{3\sin\frac{1}{2}(\alpha-\Theta)}\left[\cos^3\left(\frac{\alpha-\Theta}{2}\right) - 1\right] + \sin(\alpha-\Theta)\right\}\right]\frac{r}{a} - \frac{1}{2}\left(\frac{r}{a}\right)^2 \sin(\alpha-\Theta). \tag{A 3}$$

Appendix B

In order to quantify our method for removing the systematic distortion in $\theta(r)$, we had to establish that our 'straight edge' was indeed straight. This was accomplished by applying our distortion-removing method to an image of a static fluid interface, whose shape is known to satisfy (A 3), with θ_0 replacing Θ for present purposes. The straight edge was the glass tube used in our experiments. Figure 5 gives the difference between the above theoretical value and the experimentally measured values of θ, denoted by $\Delta\theta$, along a segment of a static interface, before and after the distortion was removed from the experimental data. The value of θ_0 was chosen to make the theory fit best, in the least-squares sense, the experimental data. Since the value of $\Delta\theta$ is less than approximately $\pm 0.2°$ after removing the distortion, we concluded that the tube was straight, at least for our purposes. Evidentally, the image of the static fluid interface was located in a region having a minimal amount of distortion.

Since the degree of distortion varied across the image, it was necessary to establish that the variation was not significant between the positions of the straight edge used to remove the distortion and that of the dynamic interfaces whose shapes were being corrected. We did this by using one image of the straight edge to remove the distortion from another image of the straight edge located at a neighbouring position and rotated slightly. This was done within that part of the field of view where the images of the fluid interface were located. The degree of separation and rotation were chosen to be somewhat larger than those corresponding to the images of the straight edges and fluid interface. Figure 6 illustrates a typical case. The large angular variation corresponding to the uncorrected image as an indication of the extent of the distortion. The small random angular variation about a horizontal line, corresponding to the corrected image, indicates the success of our method at removing the distortion.

The distortion analysed thus far represents 'short-range' distortion, the relative distortion along the segments of the fluid interface over which θ was measured in the graphs of figure 4. This follows directly from the fact that the slopes along the images of the straight edges were measured relative to the tangents at their end points closest to the centres of the prints. The 'long-range' distortion, represented by the errors in the directions of these tangents relative to a common datum, such as the true vertical, as determined with the plumb bob, was not measured beyond estimating that it did not exceed $\pm 0.5°$. Thus, our method of removing the distortion succeeded in 'straightening' the image of the straight edge illustrated in figure 6, that is to say, in eliminating the short-range distortion; however, significant long-range distortion, represented in this case by the accuracy of the value of θ of the horizontal line in the figure, 78.68°, remains, having a value of $\pm 0.5°$. This is the

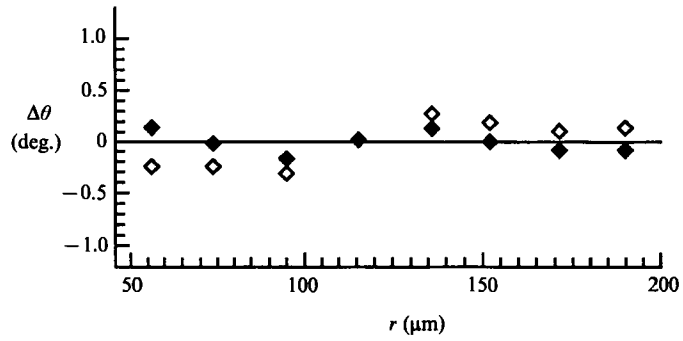

FIGURE 5. The removal of distortion in the image of a segment of a static meniscus. The differences between the theoretically predicted and experimentally measured slopes, $\Delta\theta$, before, denoted by ◇, and after, denoted by ◆, removing the distortion from the experimental data. Here, $\alpha = 65°$, $\theta_0 = 5.48°$ before, and $\theta_0 = 5.27°$ after.

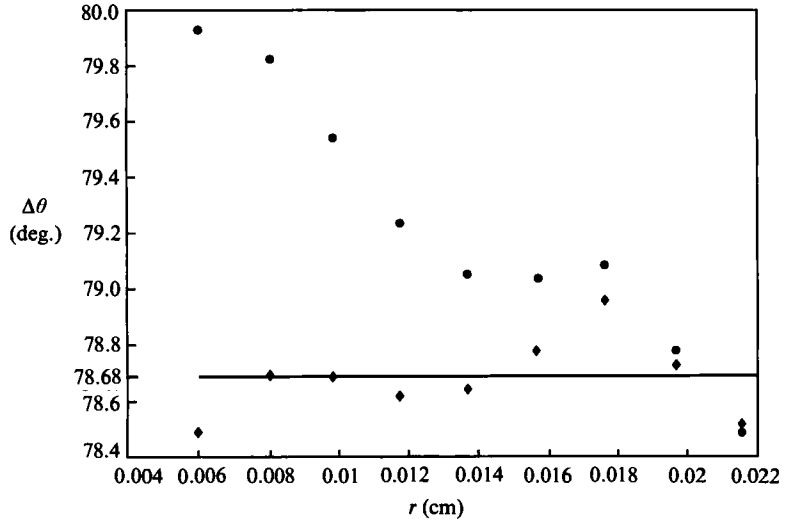

FIGURE 6. The removal of distortion in an image of a straight edge with a different image of the straight edge. The slope of the straight edge before removing the distortion is denoted by ●, and after removing the distortion by ◆.

principal reason for basing each of the graphs in figure 4 on a single image of the fluid interface, our objective being the measurement of the viscous deformation to the fluid interface, and not the attainment of archival data for this particular material system. This also accounts for our estimate of the error in measuring α.

REFERENCES

BOENDER, W. & CHESTERS, A. K. 1986 The hydrodynamics of moving contact lines: an analytic approximation for the advancing liquid-gas case, private communications.

COX, R. G. 1986 The dynamics of the spreading of a liquid on a solid surface. *J. Fluid Mech.* **168**, 169.

DURBIN, P. A. 1988 Considerations on the moving contact-line singularity, with application to frictional drag on a slender drop. *J. Fluid Mech.* **197**, 157.

DUSSAN V., E. B. 1976 The moving contact line: the slip boundary condition. *J. Fluid Mech.* **77**, 665.

GOLDSTEIN, S. 1938 *Modern Developments in Fluid Dynamics*, pp. 676–80. Oxford University Press.

HALST, H. VAN DER 1979 *Light Scattering by Small Particles*. University Microfilms International, Ann Arbor.

HOCKING, L. M. 1976 A moving fluid interface on a rough surface. *J. Fluid Mech.* **76**, 801.

HOCKING, L. M. & RIVERS, A. D. 1982 The spreading of a drop by capillary action. *J. Fluid Mech.* **121**, 425.

HUH, C. & MASON, S. G. 1977 The steady motion of a liquid meniscus in a capillary tube. *J. Fluid Mech.* **81**, 401.

HUH, C. & SCRIVEN, L. E. 1969 Shapes of axisymmetric fluid interfaces of unbounded extent. *J. Colloid Interface Sci.* **30**, 323.

JACKSON, R. 1977 *Transport in Porous Catalysts*. Elsevier.

JANSONS, K. M. 1986 Moving contact lines at non-zero capillary number. *J. Fluid Mech.* **167**, 393.

KOPLIK, J., BANAVAR, J. R. & WILLEMSEN, J. F. 1988 Molecular dynamics of Poiseuille flow and moving contact lines. *Phys. Rev. Lett.* **60**, 1282.

LOWNDES, J. 1980 The numerical simulation of the steady motion of the fluid meniscus in a capillary tube. *J. Fluid Mech.* **101**, 631.

NGAN, C. G. & DUSSAN V., E. B. 1989 On the dynamics of liquid spreading on solid surfaces. *J. Fluid Mech.* **209**, 191.

THOMPSON, P. A. & ROBBINS, M. O. 1989 Simulations of contact-line motion: slip and dynamic contact angle. *Phys. Rev. Lett.* **63**, 766.